

Magnetic field in Cepheus A as deduced from OH maser polarimetric observations

A. Bartkiewicz,^{1*} M. Szymczak,¹ R.J. Cohen² and A.M.S. Richards²

¹*Toruń Centre for Astronomy, Nicolaus Copernicus University, ul. Gagarina 11, 87-100 Toruń, Poland*

²*Jodrell Bank Observatory, University of Manchester, Macclesfield, Cheshire SK11 9DL, UK*

Released 2004 Xxxxx XX

ABSTRACT

We present the results of MERLIN polarization mapping of OH masers at 1665 and 1667 MHz towards the Cepheus A star-forming region. The maser emission is spread over a region of 6 arcsec by 10 arcsec, twice the extent previously detected. In contrast to the 22-GHz water masers, the OH masers associated with HII regions show neither clear velocity gradients nor regular structures. We identified ten Zeeman pairs which imply a magnetic field strength along the line-of-sight from -17.3 to $+12.7$ mG. The magnetic field is organised on the arcsecond scale, pointing towards us in the west and away from us in the east side. The linearly polarized components, detected for the first time, show regularities in the polarization position angles depending on their position. The electric vectors of OH masers observed towards the outer parts of HII regions are consistent with the interstellar magnetic field orientation, while those seen towards the centres of HII regions are parallel to the radio-jets. A Zeeman quartet inside a southern HII region has now been monitored for 25 years; we confirm that the magnetic field decays monotonically over that period.

Key words: masers – polarization – magnetic fields – stars: formation – ISM: individual: Cep A – molecules – radio lines: ISM – HII regions

1 INTRODUCTION

The connection between interstellar magnetic fields and the phenomenon of bipolar outflow from young stars is a topic of great observational and theoretical interest (e.g. Bachiller 1996; Ward-Thompson et al. 2000; Kudoh & Shibata 1997; and references therein). OH masers provide a useful tool for probing the kinematics and the magnetic field on subarcsecond scales, near the centres of bipolar outflows from massive young stars (Cohen 1989). The OH masers are generally found at distances from a few hundred to a few thousand au from the central source, and are sensitive to magnetic fields as small as 1 mG through the Zeeman effect. A series of OH maser studies has revealed a common pattern of OH masers tracing a dense molecular disc perpendicular to the bipolar outflow, with the magnetic field twisted in the way predicted by the magnetohydrodynamic models by Uchida & Shibata (1985) and others (Hutawarakorn & Cohen 1999, 2003, 2005; Hutawarakorn, Cohen & Brebner 2002; Gray, Hutawarakorn & Cohen 2003). The magnetic field is oriented along the outflow direction on the 10-arcsec scales probed by submm-polarimetry, but has a toroidal component wound around the outflow on the arcsec scale

probed by the OH masers. This appears in the form of a magnetic field reversal on opposite sides of the disc. In the present paper we consider the OH masers associated with the well known outflow source Cepheus A.

Cepheus A is a nearby star-forming region (within 1 kpc) and the densest part of the molecular cloud complex located to the south of the Cepheus OB3 association (Sargent 1977). The large-scale (~ 10 arcmin) morphology of this cloud seen in CO emission implies bipolar outflow at velocities of $\sim 25 \text{ km s}^{-1}$ (Rodriguez, Ho & Moran 1980). The base region of Cep A observed in the NH_3 and CO lines with angular resolutions of 2 arcsec and 15 arcsec respectively, shows a quadrupolar structure of the molecular outflow (Torrelles et al. 1993). The observations of several thermal lines confirm the presence of multiple outflows (Narayanan & Walker 1996; Codella et al. 2003). The complexity of the spatial and velocity structure of the Cep A region, characteristic of turbulent flow, is supported by maps of the H_2 emission line at $2.1 \mu\text{m}$ (Hiriart, Salas & Cruz-Gonzalez 2004). Hughes & Wouterloot (1984) found several compact HII regions (CHIIRs) at centimetre wavelengths; these mostly follow the edges of the NH_3 clouds (Torrelles et al. 1993). All of those CHIIRs are younger than 10^3 yr and some of them are likely associated with high-mass powering

* formerly Niezurawska, e-mail: annan@astro.uni.torun.pl

stars of spectral types B3 or earlier (Hughes 2001). Some CHIIRs are accompanied by clusters of OH, H₂O and CH₃OH masers (e.g. Cohen, Rowland & Blair 1984; Torrelles et al. 1996; Minier, Booth & Conway 2000). Systematic studies of OH masers with high angular resolution revealed that most OH components move away from the central CHIIRs on an estimated outflow time-scale of ~ 300 yr (Migenes, Cohen & Brebner 1992). Observations of H₂O masers indicate the presence of remarkable linear and arcuate structures, which can delineate shock fronts or discs (Torrelles et al. 1998; Torrelles et al. 2001; Curiel et al. 2002; Gallimore et al. 2003). The H₂O maser structure centred on the source HW2 is interpreted as due to a molecular disc, 600 au in diameter, which is perpendicular to the thermal radio jet. The inferred mass of the powering source is $\sim 20 M_{\odot}$, i.e. it is a B0.5 or earlier star (Torrelles et al. 1996).

In the paper we report full polarimetric observations of Cep A in the 1.6 GHz OH maser lines. Zeeman splitting of the OH maser lines at 1665- and 1667 MHz gave a value of +3.5 mG, where the plus sign indicates a field directed away from us. Another Zeeman pair has been identified in the 22-GHz water maser line; the inferred field strength is -3.2 mG (Sarma et al. 2002), that is, pointing towards us. Such magnetic fields are believed to have a non-negligible dynamical effect (Migenes et al. 1992). We attempt to extend previous the observations by using new polarization data to obtain an overall structure of magnetic field in the central region of Cep A.

2 OBSERVATIONS AND DATA REDUCTION

Cep A was observed in 1999 in all four ground-state OH transitions using 6 telescopes of the Multi-Element Radio Linked Interferometer Network (MERLIN) (Table 1). Each transition was observed in left- (LHC) and right-circular polarization (RHC) simultaneously and correlated to obtain all four Stokes parameters. The spectral bandwidth of 250 kHz, covering a velocity range of 45 km s^{-1} , was divided into 128 channels, yielding a channel spacing of 0.35 km s^{-1} . The band centre was set to a local standard of rest (LSR) velocity of -14 km s^{-1} .

The phase-referencing technique was applied at all epochs with the continuum source 2300+638 used as a phase-calibrator. Since the reference source was too weak to be observed in narrow-band mode, it was observed in wide-band mode (16-MHz) at the appropriate frequencies (given in Table 1) to achieve the optimum signal-to-noise ratio. The cycle-times between Cep A and the reference were 5.5 min+2 min at the main line transitions and 6.5 min+2 min at the satellite line transitions. In addition 3C286 and 3C84 were observed for 1-3 hours in all sessions, at the relevant narrow and wide-band frequencies corresponding to the frequencies given in Table 1 (corrected to the appropriate V_{LSR} for the narrow-band configurations). 3C286 was used as the primary calibrator for the flux density scale and for the polarization angle; 3C84 was used as the point source, bandpass calibrator and for the polarization leakage corrections.

Data reduction was carried out using standard procedures (Diamond et al. 2003) with the local **d-programs** at

Jodrell Bank and the Astronomical Image Processing System (AIPS). To map the emission we used a circular Gaussian beam of full width half maximum (FWHM) 120 mas and the pixel separation was 40 mas in all epochs of observations (the synthesised beams for all data are given in Table 1). The rms noise (σ) levels in emission-free Stokes *I* single channel maps were typically a few mJy beam⁻¹ (Table 1). The 1665-MHz data taken on May 20 were affected by the ringing effect. This data set was therefore smoothed using a Hanning function.

A region of 20 arcsec by 20 arcsec centred at RA= $22^{\text{h}}56^{\text{m}}18^{\text{s}}.033$, Dec= $62^{\circ}01'48''.347$ (J2000) was inspected for total intensity emission (*I* Stokes parameter) stronger than 5σ . We fitted 2 dimensional Gaussian components to each patch of maser emission in each channel to measure its position and flux density. The emission was considered to be real if present at least in three contiguous channels. We measured the flux densities in the images of the other Stokes parameters at the position of each *I* Stokes component, using the local AIPS task MFQUV. We grouped series of components above 5σ arising from similar positions in successive channels into features and analysed them. More details on data reduction procedures and determination of the uncertainties in the maser positions were given by Niezurawska et al. (2004).

3 RESULTS

3.1 Polarization spectra

Spatially complex OH maser emission was found at 1665 and 1667 MHz in the velocity ranges from -26 to 0.1 km s^{-1} and from -16 to -3 km s^{-1} , respectively. The spectra of the LHC and RHC polarizations and the linear polarization ($P = (Q^2 + U^2)^{0.5}$) are presented in Fig. 1. No significant differences were noted in the spectra at the two epochs spanned by 10 days. Our circularly polarized spectra differ considerably from those reported in Cohen et al. (1984). However, Cep A is noted for OH flare activity and strong variability (Cohen & Brebner 1985).

No 1612-MHz emission was detected above a level of 15 mJy over the whole region searched at both epochs. This is consistent with single dish observations by Cohen, Brebner & Potter (1990) who found weak and broad 1612-MHz emission which was resolved-out by MERLIN.

The 1720-MHz emission appeared on 1999 May 20 as completely circularly polarized features with a peak intensity of about 1 Jy (Fig. 1) which decreased by a factor of two after four weeks (Niezurawska et al. 2004). We did not detect any linear polarization at that transition within a sensitivity limit of 15 mJy.

3.2 Distribution of the maser components

All OH maser features above 5σ level are listed in Table 2 and plotted in Fig. 2. In total, we detected 49 OH masers at 1.6 GHz lines, 31 features are new (marked with superscript *n* in Table 2) and 18 were seen previously (Cohen et al. 1984; Migenes et al. 1992; Argon, Reid & Menten 2000). The 6 arcsec by 10 arcsec region contains 25 LHC and 16 RHC

Table 1. Details of the MERLIN observations.

Date	Line transition (MHz)	Phase calibrator		Synthesised beam		Time on source (h)	Rms noise per channel (mJy b ⁻¹)
		Frequency (MHz)	Flux density (mJy)	HPBW (mas)	P.A. (°)		
20 May 1999	1612.231	1612.4	124	180×140	−27	7.5	3
	1665.402	1661.2	128	149×120	−7	6.4	5
	1667.359	1661.2	125	148×119	−11	6.4	4
	1720.530	1720.8	130	154×107	−24	7.6	3
30 May 1999	1665.402	1661.2	128	136×123	2	5.2	3
	1667.359	1661.2	130	136×122	−5	5.1	4
16 June 1999	1612.231	1612.4	124	165×115	−33	3.7	4
	1720.530	1720.8	150	143×109	−32	3.7	4

Antennas: Defford, Cambridge, Knockin, Darnhall, Mark II, Tabley

Table 2. Positions of OH masers in Cep A observed on 1999 May 30. The newly detected components are marked with superscript *n*. The numbers in brackets indicate relative errors in positions (×0⁰.0001 for RA, ×0⁰.001 for Dec).

V _{LSR} (km s ⁻¹)	RA (22 ^h 56 ^m)	Dec (62°01′)	S _p (Jy b ⁻¹)	Feature	V _{LSR} (km s ⁻¹)	RA (22 ^h 56 ^m)	Dec (62°01′)	S _p (Jy b ⁻¹)	Feature
1665-MHz LHC					1665-MHz RHC				
−25.2 ⁿ	18 ^s 1642(2)	49′′668(2)	0.285	A	−18.0 ⁿ	18 ^s 1646(3)	49′′673(2)	0.174	a
−16.1 ⁿ	18 ^s 0771(2)	45′′809(8)	0.296	B	−14.2	18 ^s 1143(1)	46′′316(1)	5.240	b
−16.1 ⁿ	17 ^s 9472(3)	49′′829(3)	0.779	C	−14.2 ⁿ	17 ^s 9474(4)	49′′839(3)	0.359	c
−16.1	18 ^s 1148(1)	46′′320(1)	8.880	D	−13.1	18 ^s 0976(2)	49′′343(2)	0.359	d
−14.4 ⁿ	18 ^s 1383(2)	46′′466(1)	3.335	E	−12.3 ⁿ	18 ^s 1464(3)	47′′030(3)	0.301	e
−13.9 ⁿ	18 ^s 1324(1)	46′′494(1)	16.250	F	−11.9 ⁿ	18 ^s 2134(15)	46′′510(13)	0.066	f
−13.9 ⁿ	18 ^s 0951(8)	45′′964(6)	0.579	G	−11.7 ⁿ	17 ^s 9699(6)	50′′012(5)	0.130	g
−13.9	17 ^s 9651(3)	50′′006(2)	1.426	H	−11.6 ⁿ	18 ^s 1352(1)	46′′487(1)	2.070	h
−12.3	17 ^s 8382(2)	48′′675(1)	0.622	I	−11.5	17 ^s 8662(5)	48′′812(4)	0.196	i
−11.5	17 ^s 8656(2)	48′′813(1)	2.224	J	−11.2 ⁿ	17 ^s 8843(1)	46′′508(1)	0.515	j
−11.4 ⁿ	17 ^s 6966(7)	52′′311(6)	0.195	K	−8.0	17 ^s 9978(5)	49′′678(4)	0.131	k
−8.7 ⁿ	17 ^s 7184(6)	49′′999(5)	0.216	L	−7.0	17 ^s 9084(5)	50′′6132(5)	0.090	l
−8.6	17 ^s 8852(1)	46′′484(1)	2.630	M	−2.8 ⁿ	17 ^s 9985(4)	49′′667(3)	0.135	m
−7.9	17 ^s 9947(1)	49′′682(1)	5.192	N	−0.6 ⁿ	17 ^s 9111(11)	49′′361(7)	0.423	n
−7.9 ⁿ	17 ^s 8273(4)	53′′190(3)	0.471	O	−0.6 ⁿ	17 ^s 9498(1)	49′′843(1)	15.370	o
−7.8 ⁿ	18 ^s 3843(12)	47′′314(10)	0.098	P	−0.6 ⁿ	17 ^s 7829(3)	53′′363(3)	1.097	p
−7.7 ⁿ	17 ^s 9582(11)	49′′175(6)	0.209	Q					
−6.7 ⁿ	17 ^s 9478(2)	49′′868(1)	0.583	R					
−6.2	18 ^s 1163(1)	49′′386(1)	4.590	S					
−6.2 ⁿ	17 ^s 9488(4)	52′′906(3)	0.374	T					
−6.1 ⁿ	17 ^s 8903(7)	46′′497(5)	0.156	U					
−6.1 ⁿ	18 ^s 0778(9)	48′′881(6)	0.167	V					
−4.9	18 ^s 0497(2)	47′′552(1)	0.481	W					
−2.4 ⁿ	17 ^s 8407(2)	49′′898(2)	0.293	Y					
−0.7	17 ^s 9520(7)	49′′848(5)	0.109	Z					
1667-MHz LHC					1667-MHz RHC				
−15.7 ⁿ	18 ^s 3852(4)	42′′737(3)	0.936	A	−14.6	18 ^s 1123(1)	46′′306(1)	3.962	a
−15.7	18 ^s 1125(1)	46′′305(1)	4.831	B	−5.4	17 ^s 8358(2)	49′′912(2)	0.611	b
−3.1 ⁿ	18 ^s 1096(4)	46′′334(4)	0.580	C					
−3.1	17 ^s 8372(1)	49′′899(1)	2.907	D					
1720-MHz LHC					1720-MHz RHC				
−13.3 ⁿ	17 ^s 6124(1)	44′′533(1)	1.2354	A	−15.4 ⁿ	17 ^s 6147(1)	44′′517(1)	1.122	a

features in the 1665 MHz line, four LHC and two RHC features in the 1667 MHz line and single LHC and RHC features in the 1720 MHz line.

For the assumed distance of 725 pc (Blaauw, Hiltner & Johnson 1959) the projected area containing OH maser emission is 4350×7250 au² i.e. about

twice as great as that reported previously. The masers are mostly projected against HII regions labelled as 2, 3b, 3c (the nomenclature of Hughes & Wouterloot (1984)) and 3di, 3dii, 3diii regions resolved by Torrelles et al. (1998). Note that we use the convention presented by Torrelles et al. (1998) in their Table 1 but not in their Fig. 1.

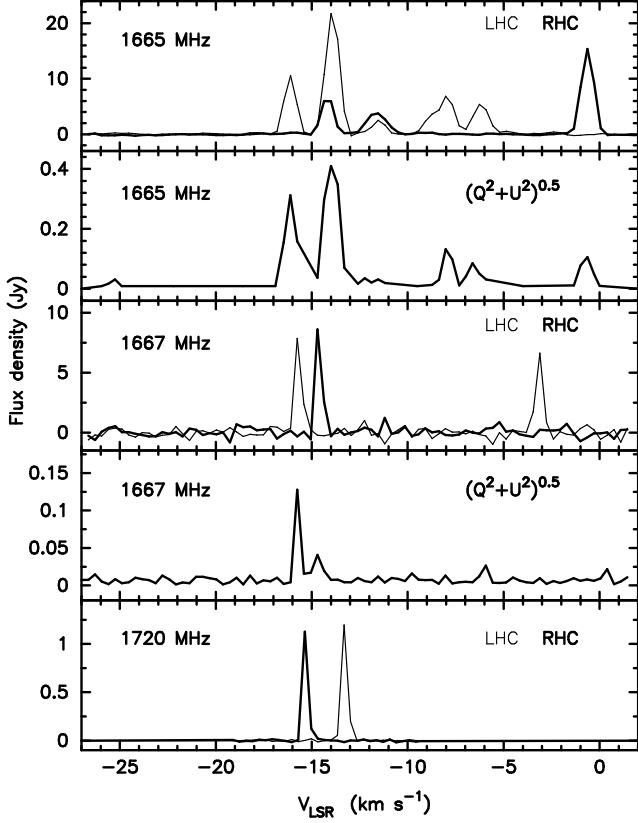


Figure 1. The spectra of Cep A taken with MERLIN in May 1999. OH main-line spectra are averaged from two epochs (20 and 30 May). The bottom panel shows the 1720-MHz emission detected in 20 May 1999.

24 OH maser features at 1665- and 1667-MHz are centred around the HII region 2 within the velocity range from -25.2 km s^{-1} to -0.6 km s^{-1} . 14 OH features from both transitions with velocities from -16.1 km s^{-1} to -3.1 km s^{-1} were projected towards the continuum sources 3di, 3dii, 3diii. Three OH 1665-MHz features with velocities -11.2 , -8.6 , -6.1 km s^{-1} were close the east edge of the HII region 3c. Six features, which all were detected for the first time, are not obviously associated with any known continuum source. Four 1665-MHz masers with LSR velocities of -11.4 , -7.9 , -6.2 and -0.6 km s^{-1} are located 3.8 arcsec northward of the continuum source 2. One 1665-MHz feature with an LSR velocity of -7.8 km s^{-1} lies about 2 arcsec NW of the 3dii centre, while one 1667-MHz feature, at -15.7 km s^{-1} , is placed 3.8 arcsec southward of the source 3dii (Fig. 2). Two 1720-MHz features are projected towards the southern edge of source 3b and coincide with the OH 4765-MHz emission which we reported in Niezurawska et al. (2004).

3.3 Polarization properties and magnetic field

We found ten Zeeman pairs with features coinciding spatially within 36 mas. Table 3 summarizes their properties. Seven pairs were found at 1665 MHz, two at 1667 MHz and one at 1720 MHz. Five of them, named Z_1 , Z_2 , Z_3 , Z_4 and Z_8 are located around the HII region 2. Three pairs, Z_6 , Z_7 (1665 MHz) and Z_7 (1667 MHz), are projected at the sources

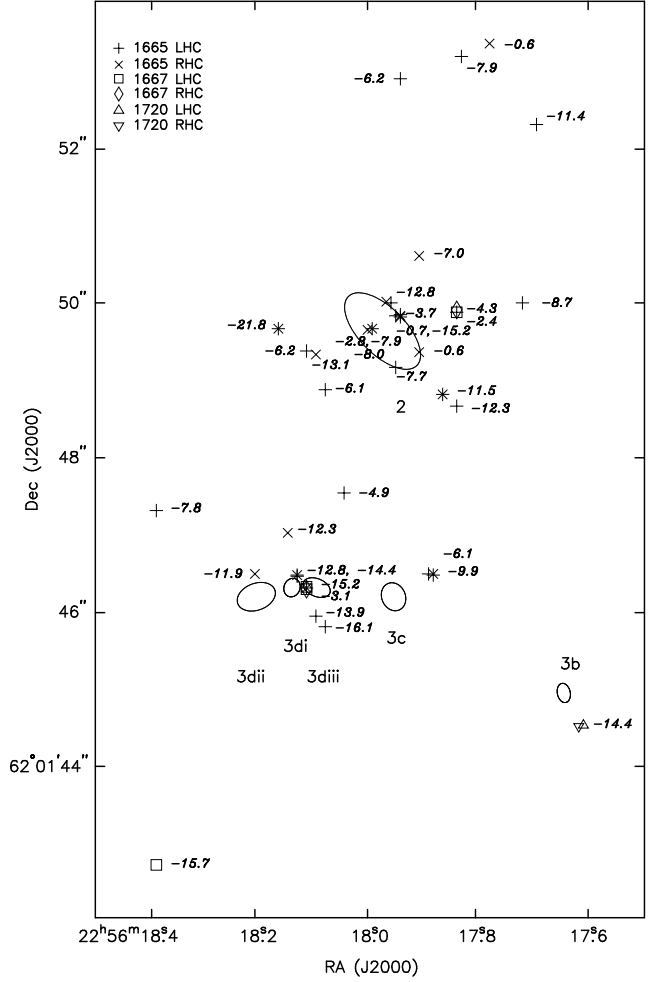


Figure 2. The OH maser distribution in the Cep A region measured with MERLIN. Symbols trace the 1665-, 1667- and 1720-MHz LHC and RHC features as indicated in the top-left corner. Each feature is labelled by its central LSR velocity (italic numbers). In a case of Zeeman pairs the demagnetized velocity is given. Ellipses trace the continuum sources (Torrelles et al. 1998). Upright numbers label the continuum sources according to Hughes & Wouterloot (1984) and Torrelles et al. (1998).

3di and 3diii. Pair Z_5 lies close to the region 3c, whereas the only one Zeeman pair at 1720 MHz line appears in the vicinity of the HII region 3b. We calculated the magnetic field strength (B) from the velocity separation of the Zeeman components (ΔV) using coefficients taken from Table 2 in Davies (1974). However, as we stated in Niezurawska et al. (2004), in the case of 1720-MHz transition we assumed that the emission came from well-separated σ^{+1} and σ^{-1} components and used the line splitting of $118 \text{ km s}^{-1} \text{ G}^{-1}$.

Two Zeeman pairs, one at 1665 MHz and one at 1667 MHz, labelled as Z_7 , coincide spatially and in velocity. In the past they were reported by Wouterloot, Habing & Herman (1980) as a Zeeman quartet. Channel maps of that quartet in linearly polarized emission are shown in Fig. 3 and the polarization profiles in Fig. 4. The emission at -15.8 km s^{-1} appears at both transitions with similar linear polarized flux densities, $P \approx 145 \text{ mJy b}^{-1}$, while the polarization angles differ significantly by 23° . We think that blending of features

Table 3. 1.6-GHz Zeeman pairs found in Cep A. The peak flux densities (S_p), the separation in velocity (ΔV) between two features of opposite circular polarization, the demagnetized velocities (V_d) of those features and calculated magnetic field strengths (B) are given. The negative sign corresponds to the field towards the observer. The last column identifies features according to the nomenclature from Table 1.

	Polzn.	RA (22 ^h 56 ^m)	Dec (62°01′)	V_{LSR} (km s ⁻¹)	S_p (Jy b ⁻¹)	ΔV (km s ⁻¹)	V_d (km s ⁻¹)	B (mG)	
1665-MHz									
Z₁	LHC	17 ^h 9651	50′006	-13.9	1.426	-2.2	-12.8	3.7	H
	RHC	17 ^h 9699	50′012	-11.7	0.130				g
Z₂	LHC	17 ^h 9478	49′868	-6.7	0.583	-6.1	-3.7	10.3	R
	RHC	17 ^h 9498	49′843	-0.6	15.370				o
Z₃	LHC	17 ^h 9472	49′829	-16.1	0.779	-1.9	-15.2	3.2	C
	RHC	17 ^h 9474	49′839	-14.2	0.360				c
Z₄	LHC	18 ^h 1642	49′668	-25.5	0.285	-7.5	-21.8	12.7	A
	RHC	18 ^h 1646	49′673	-18.0	0.174				a
Z₅	LHC	17 ^h 8852	46′484	-8.6	2.630	2.6	-9.9	-4.4	M
	RHC	17 ^h 8843	46′508	-11.2	0.515				j
Z₆	LHC	18 ^h 1324	46′494	-13.9	16.250	-2.3	-12.8	3.9	F
	RHC	18 ^h 1352	46′487	-11.6	2.070				h
Z₇	LHC	18 ^h 1148	46′320	-16.1	8.880	-1.9	-15.2	3.2	D
	RHC	18 ^h 1143	46′316	-14.2	5.240				b
1667-MHz									
Z₈	LHC	17 ^h 8372	49′899	-3.1	2.907	2.3	-4.3	-6.5	D
	RHC	17 ^h 8358	49′912	-5.4	0.611				b
Z₇	LHC	18 ^h 1125	46′305	-15.7	4.831	-1.1	-15.2	3.1	B
	RHC	18 ^h 1123	46′306	-14.6	3.962				a
1720-MHz									
Z₉	LHC	17 ^h 6124	44′533	-13.3	1.050	2.1	-14.4	-17.3	A
	RHC	17 ^h 6147	44′517	-15.4	1.122				a

unresolved by MERLIN is the most likely explanation for that difference (see Fig. 3 and compare e.g. panels $V_{LSR} = -14.7 \text{ km s}^{-1}$ at both transitions). Moreover, the single dish spectra of the quartet showed asymmetries in the line profiles, i.e. more than one Gaussian component was needed for an accurate fit (Cohen et al. 1990).

Table 4 gives the polarization characteristics of all maser features detected in 1999; the LSR velocity, the J2000 coordinates together with their errors, the I, Q, U, V and P flux densities, the polarization position angle $\chi = 0.5 \times \arctan(U/Q)$ and its error σ_χ , the percentage of linear polarization, $m_l = (Q^2 + U^2)^{0.5}/I$, the percentage of circular polarization, $m_c = V/I$ and the percentage of total polarization, $m_t = (m_c^2 + m_l^2)^{0.5}$. The random errors σ_χ due to thermal noise were calculated according to the formula $\sigma_\chi = 0.5 \times \sigma_P / P \times 180^\circ / \pi$ (Wardle & Kronberg 1974). The errors arising from uncertainty in the measurement of the polarization angle of 3C286 were 4° and 3° at 1665 and 1667 MHz respectively. These systematic errors do not affect comparisons within the same data set, so they are not included in Table 4.

We found 14 linearly polarized OH maser features

at 1665 MHz and two at 1667 MHz above the 5σ level ($P \geq 0.010 \text{ mJy}$). Even when linear polarization is detected in Cep A the percentage polarization is generally low (≤ 16 percent); we detected only two 1665-MHz components with m_l of 22 and 31 percent. In contrast, the circular polarization percentages are typically higher with a median value of 77 percent and with two cases fully polarized, in 1665 MHz line. Similarly, the 1667-MHz line shows ≤ 6 percent linear polarization but almost full circular polarization with a median value $m_c = 90$ percent. The distribution of linearly polarized components together with their polarization characteristic are presented in Fig. 5. We did not find any linear polarization in the 1720-MHz transition above the 5σ limit.

4 DISCUSSION

4.1 OH masers and radio continuum sources

The present study reveals that the OH masers are spread over an area of 6 arcsec by 10 arcsec. In addition to two main clusters of maser components (Cohen et al. 1984)

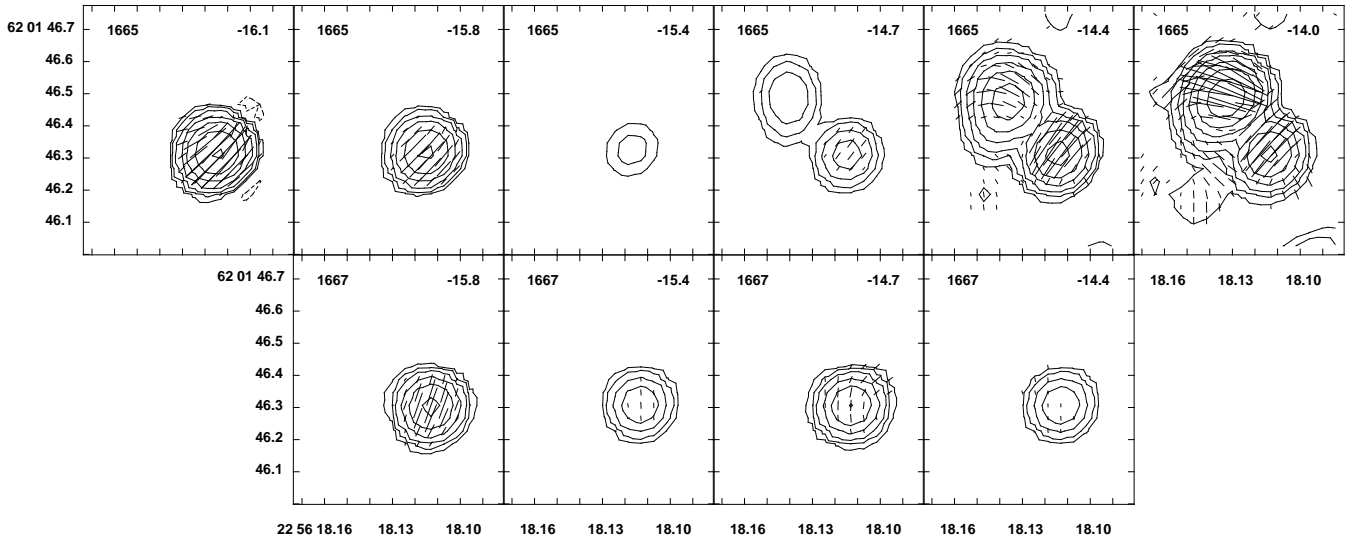


Figure 3. Channel maps of linear polarization of the Zeeman quartet at 1665 and 1667 MHz. Contour levels are $-1, 1, 2, 4, \dots \times 60 \text{ mJy b}^{-1}$. LSR velocities are indicated at the upper-left corners. Bars show the orientation of the electric vectors and have lengths proportional to the linearly polarized intensities where $0.1 \text{ arcsec} = 125 \text{ mJy b}^{-1}$.

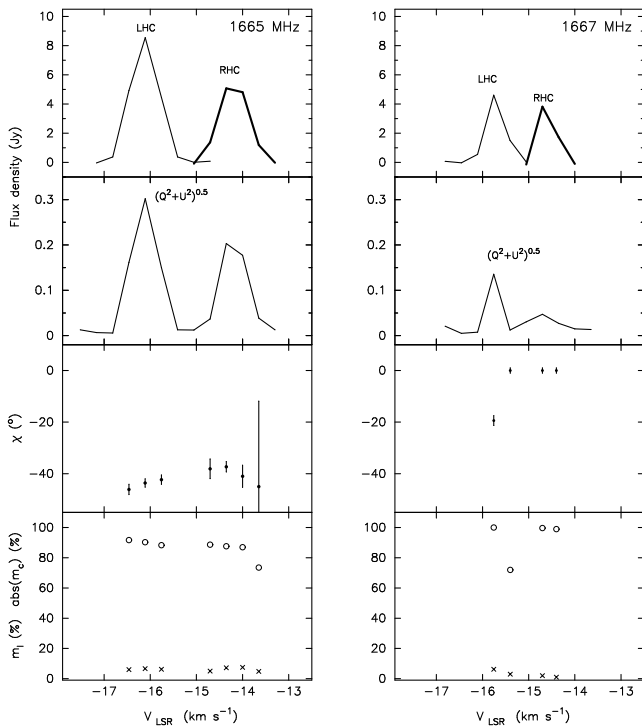


Figure 4. Polarization profiles of the OH Zeeman quartet in Cep A at 1665 and 1667 MHz. In the lowest panel the circle and cross symbols correspond to m_c and m_l , respectively.

associated with the radio continuum sources 2 and 3 (Hughes & Wouterloot 1984) we detected several components which have not been reported before and which are not accompanied by radio continuum background. 94 per cent of the new components are much brighter than the 0.1 Jy sensitivity limit of previous observations, demonstrating the high variability of OH masers.

OH 1665-MHz masers around region 2 (which has a complex structure) encompass a wider range of veloci-

ties (-25.2 km s^{-1} to -0.6 km s^{-1}) than that reported by Cohen et al. (1984). This maser complex extends 3 arcsec (2175 au) in an E-W direction and its geometrical centre is at $\text{RA}=22^{\text{h}}56^{\text{m}}17^{\text{s}}.9609$, $\text{Dec}=62^{\circ}01'49''.578$ (J2000). That gives a distance of 147 mas (107 au) from the geometrical centre of a disc traced by water masers (Torrelles et al. 1996). Although the E-W elongations of the OH and the water masers are similar, the position-velocity diagram for OH masers (after demagnetization of the velocities to compensate for Zeeman splitting) does not show the regularity expected from a disc scenario. Our results imply that the existing disc has to be strongly disturbed at the distances 1-2 arcsec from the centre of region 2 by the expanding material. In fact, there are molecular outflows at the edge (about 1 arcsec from the centre) of region 2 (Migenes et al. 1992).

The OH 1665- and 1667-MHz masers projected against the southern continuum source 3d cover mainly a velocity range from -16.1 km s^{-1} to -11.6 km s^{-1} . However, we found a highly red-shifted component of velocity -3.1 km s^{-1} . Torrelles et al. (1998) resolved 3d into a chain of four individual 22 GHz continuum sources. They point to 3dii as harbouring a young stellar object. We only detected OH maser emission from the west side of this source. If this was powered by an outflow we would expect to see a velocity gradient or a systematic spatial distribution of the masers but this was not apparent even after demagnetization of the component velocities. Torrelles et al. (1998) reported a similar situation for the water masers around that region, there were neither clear spatial nor velocity trend in distribution of maser spots.

4.2 Magnetic field

The most important result of our polarimetric observations concerns the overall regularity of the magnetic field in Cep A. Fig. 5 shows the distribution of maser components with polarization information. The magnetic field, derived from the Zeeman splitting of OH 1665- and 1667-MHz lines,

Table 4. The linearly polarized OH 1665-MHz and 1667-MHz maser components in Cep A. The errors are given in brackets and are $\times 0.0001$ sec for RA, $\times 0.001$ arcsec for Dec and in degrees for χ . The last column identifies features according to the nomenclature from Table 1.

V_{LSR} (km s $^{-1}$)	RA (22 ^h 56 ^m)	Dec (62°01′)	I (Jy b $^{-1}$)	Q (Jy b $^{-1}$)	U (Jy b $^{-1}$)	V (Jy b $^{-1}$)	P (Jy b $^{-1}$)	χ (°)	m_l (%)	m_c (%)	m_t (%)	
1665-MHz												
−25.3	18 ^h 1647(4)	49′′667(3)	0.141	−0.031	−0.006	−0.132	0.031	−85(3)	22	−94	97	A
−18.0	18 ^h 1646(3)	49′′673(3)	0.083	0.002	0.002	0.066	0.003	—	0	80	80	a
−16.1	17 ^h 9471(6)	49′′827(4)	0.393	<0.002	<0.002	−0.337	<0.002	—	0	−86	86	C
−16.1	18 ^h 0773(17)	45′′804(12)	0.172	<0.002	−0.018	−0.091	0.018	−45(3)	11	−53	54	B
−16.1	18 ^h 1145(1)	46′′318(2)	4.483	0.015	−0.293	−4.049	0.294	−44(1)	7	−90	90	D
−14.4	18 ^h 1138(1)	46′′313(2)	2.661	0.051	−0.184	2.331	0.191	−37(2)	7	88	88	b
−14.0	17 ^h 9654(4)	50′′313(4)	0.678	<0.002	<0.002	−0.491	<0.002	—	0	−72	72	H
−14.0	18 ^h 0949(8)	45′′985(9)	0.334	<0.002	<0.002	−0.106	<0.002	—	0	−31	31	G
−14.0	18 ^h 1420(13)	46′′426(34)	0.708	−0.046	<0.002	−2.420	0.046	90(2)	7	−100	100	E
−13.6	18 ^h 1309(1)	46′′494(2)	6.923	−0.274	0.179	−6.176	0.328	73(2)	5	−89	90	F
−13.0	18 ^h 0979(2)	49′′346(2)	0.182	0.004	−0.006	0.150	0.007	—	0	83	83	d
−12.6	18 ^h 1459(7)	47′′029(6)	0.101	−0.006	−0.015	0.056	0.016	−55(4)	16	55	57	e
−12.2	17 ^h 8379(2)	48′′674(2)	0.314	<0.002	−0.003	−0.233	0.003	—	0	−74	74	I
−11.9	17 ^h 9705(7)	50′′032(9)	0.058	<0.002	<0.002	0.040	<0.002	—	0	68	68	g
−11.9	18 ^h 1379(2)	46′′499(2)	1.019	<0.002	−0.021	0.763	0.021	−45(5)	2	75	75	h
−11.5	17 ^h 8657(2)	48′′810(2)	1.225	<0.002	<0.002	−0.775	<0.002	—	0	−63	63	J
−11.2	17 ^h 8845(2)	46′′507(2)	0.240	0.009	<0.002	0.207	0.009	—	0	86	86	j
−8.7	17 ^h 8848(1)	46′′487(2)	1.354	−0.013	<0.002	−1.094	0.013	90(5)	1	−81	81	M
−8.0	17 ^h 9953(1)	49′′681(2)	2.681	0.086	−0.100	−2.208	0.132	−25(1)	5	−82	82	N
−8.0	17 ^h 9593(20)	49′′172(14)	0.079	<0.002	−0.009	−0.059	0.009	—	0	−75	75	Q
−8.0	17 ^h 8275(5)	53′′189(6)	0.229	<0.002	<0.002	−0.195	<0.002	—	0	−85	85	O
−7.0	17 ^h 9085(9)	50′′648(8)	0.131	−0.041	−0.004	<0.002	0.041	−87(2)	31	0	31	l
−6.6	17 ^h 9478(2)	49′′867(2)	0.300	−0.005	<0.002	−0.285	0.005	—	0	−95	95	R
−6.3	18 ^h 1167(1)	49′′383(2)	2.326	−0.035	0.037	−1.884	0.050	67(2)	2	−81	81	S
−6.3	18 ^h 0788(10)	48′′872(10)	0.091	<0.002	<0.002	−0.072	<0.002	—	0	−79	79	V
−6.3	17 ^h 9492(6)	52′′905(7)	0.190	<0.002	<0.002	−0.142	<0.002	—	0	−75	75	T
−5.9	17 ^h 8907(8)	46′′496(9)	0.088	<0.002	<0.002	−0.058	<0.002	—	0	−66	66	U
−4.9	18 ^h 0496(2)	47′′550(2)	0.233	<0.002	<0.002	−0.211	<0.002	—	0	−90	90	W
−2.4	17 ^h 8410(3)	49′′899(3)	0.146	0.003	<0.002	−0.127	0.003	—	0	−87	87	Y
−1.0	17 ^h 9122(24)	49′′354(15)	0.089	<0.002	−0.010	0.102	0.010	−45(6)	11	100	100	n
−0.6	17 ^h 9499(5)	49′′842(5)	7.761	−0.025	−0.102	6.852	0.106	−52(1)	1	88	88	o
−0.6	17 ^h 7829(4)	53′′362(5)	0.535	<0.002	<0.002	0.442	<0.002	—	0	83	83	p
1667-MHz												
−15.8	18 ^h 1125(1)	46′′303(2)	2.324	0.111	−0.090	−2.422	0.143	−19(1)	6	−100	100	B
−15.7	18 ^h 3852(4)	42′′737(3)	0.482	<0.002	<0.002	−0.455	<0.002	—	0	−94	94	A
−14.7	18 ^h 1123(1)	46′′306(2)	1.937	0.039	<0.002	1.932	0.039	0(2)	2	100	100	a
−5.4	17 ^h 8358(2)	49′′912(2)	0.334	<0.002	<0.002	0.281	<0.002	—	0	84	84	b
−3.1	18 ^h 1096(4)	46′′334(4)	0.397	−0.008	<0.002	−0.261	0.008	—	0	−66	66	C
−3.1	17 ^h 8372(1)	49′′899(1)	1.481	<0.002	<0.002	−1.412	<0.002	—	0	−95	95	D
1720-MHz												
−15.4	17 ^h 6147(1)	44′′517(1)	0.531	<0.002	<0.002	0.525	<0.002	—	0	99	99	a
−13.3	17 ^h 6124(1)	44′′533(1)	0.507	<0.002	<0.002	0.561	<0.002	—	0	−100	100	A

is negative (pointed towards us) in the west and positive (pointed away from us) in the east side of the mapped region. Sarma et al. (2002) detected a Zeeman pair in the water maser line at 22 GHz and derived an upper limit to the field strength of -3.2 mG. That component lies just on the west side of Cep A and is consistent with the magnetic field configuration inferred from OH masers (Fig. 5). Furthermore, a Zeeman pair found in the 1720-MHz OH line (Niezurawska et al. 2004) in the SW region of the mapped area supports this picture of an organised magnetic field on arcsecond scales.

The magnetic field reversal in Cep A is clearer than the reversals found in the molecular outflow sources stud-

ied with MERLIN by Hutawarakorn & Cohen (1999, 2003, 2005) and Hutawarakorn et al. (2002). However it is more difficult to relate the organised magnetic field structure seen in Cep A on the 1 arcsec scale to the diverse outflows seen on larger scales from ~ 1 to 3 arcmin. Table 5 lists the main molecular structures reported towards Cep A. There are four preferred directions: -45° , 0° , $+45^\circ$ and $+90^\circ$. Only H₂S shows an outflow at 0° in the expected direction orthogonal to the magnetic field reversal according to the model by Uchida & Shibata (1985). The multiplicity of outflow directions suggests that there may be several sources powering them. The present OH maser observations suggest that Cep A contains at least two active centres. There is a clear need for sensitive molecular observations at the arcsec scale

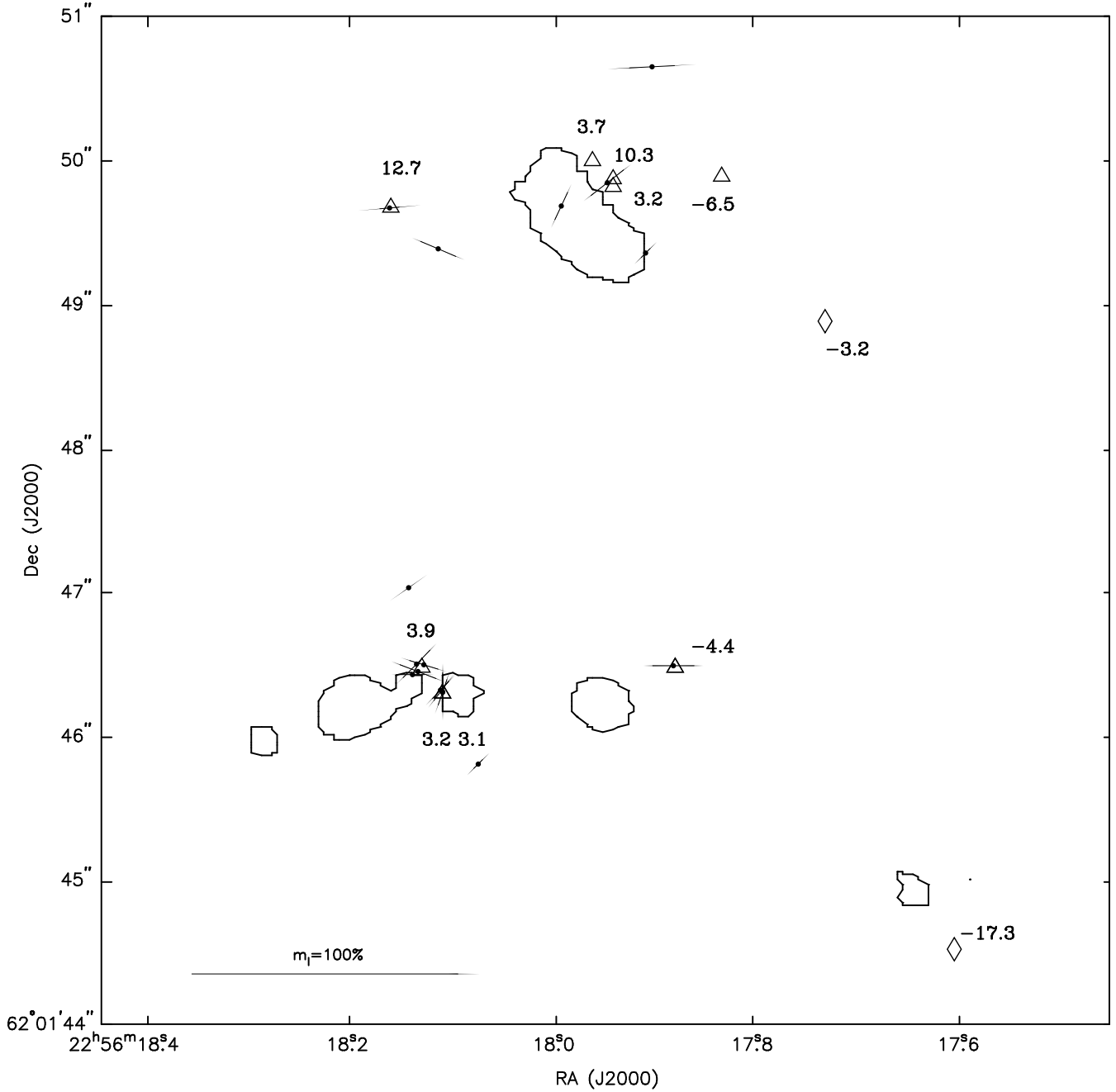


Figure 5. An overview of the magnetic field in Cep A detected using MERLIN. Numbers indicate the magnetic field strength in mG. The directions of the planes containing the electric field vectors are marked by bars with lengths proportional to the percentage linear polarization of each feature. Triangles trace the OH 1665- and 1667-MHz Zeeman pairs from this paper. Diamonds show the water maser Zeeman pair from Sarma et al. (2002) and OH 1720-MHz Zeeman pair (Niezurawska et al. 2004). The contours are at 0.5 mJy b^{-1} (3 per cent of the peak intensity) of the 22-GHz continuum emission (Torrelles et al. 1998).

which could disentangle the outflows from the complex region at the core of Cep A.

The electric vectors of linearly polarized features show a systematic trend. The polarization position angles χ of components observed in the direction of the outer parts of the HII regions are significantly rotated relative to those observed towards the centres (Fig. 5). The flux-averaged χ of the six electric vectors from the outer parts is $-87^\circ \pm 3^\circ$, which implies that the component of the magnetic field

vector in the plane of the sky has a direction of $3^\circ \pm 3^\circ$. That is closely aligned with the interstellar magnetic field orientation (-10°) derived from the infrared polarimetry towards the regions 2 and 3 (Jones, Woodward & Kelley 2004). The flux averaged χ from the centre of northern region 2 is $-37^\circ \pm 1^\circ$, which gives $53^\circ \pm 1^\circ$ for the magnetic field orientation in that area. That is parallel to the radio jet seen at 22 GHz (P.A.= 44°) (Torrelles et al. 1996). The flux averaged χ of 1665-MHz features in southern regions 3di

Table 5. Structures in Cep A regions.

Line	Scale (arcsec)	P.A. (°)	Synthesised beam (″)	Note	Reference
NH ₃	42×30 96×24 48×36	−45 +45 −135	5.4×5.3		Torrelles et al. (1993)
¹² CO	300 180	+90 +85	9.9×6.3	HV outflow EHV outflow	Narayanan & Walker (1996)
CS	91	−45		core	
HCO ⁺	60	+57	3.2×2.6	outflow	Gómez et al. (1999)
SiO	120	−33	4.7×3.7	disc	
H ₂ S	85 171 ~60	+135 +180 +45	14	HV outflow HV outflow LH outflow	Codella et al. (2003)
SO ₂	114×29	+45	24		

and 3diii (labels as in Fig. 2) are $78^\circ \pm 2^\circ$ and $-41^\circ \pm 2^\circ$, respectively. Those imply average magnetic field directions of $-12^\circ \pm 2^\circ$ and $49^\circ \pm 2^\circ$, respectively.

4.2.1 Physical conditions

The magnetic field and the gas density relationship in Cep A region was established to be $B \sim n^{0.4}$ (Garay et al. 1996). At the edge of NH₃ molecular clouds in Cep A, Garay et al. (1996) found a magnetic field strength of 0.3 mG and a number density of $2 \times 10^4 \text{ cm}^{-3}$. In this paper, we find that the magnetic field strength deduced from OH Zeeman splitting has a magnitude of 3.2 to 17.3 mG. This leads to derived gas densities in the range from 8×10^6 to $5 \times 10^8 \text{ cm}^{-3}$. Such numbers are typical for OH masers in star-forming regions, according to the model of Gray, Doel & Field (1991). Additionally, this model predicts that in the case of accelerative fields with velocity shifts of $2\text{--}3 \text{ km s}^{-1}$ the 1665-MHz line dominates at all number densities. In fact, the masing region in Cep A expands with a velocity of 2.5 km s^{-1} (Cohen et al. 1990) and the 1665-MHz emission does appear at least twice as strong as the 1667-MHz line (Fig. 1).

Hutawarakorn & Cohen (2003) suggested that the evolutionary path of star-forming regions is seen in their polarization characteristics. They detected a systematic increase in the degree of polarization from the oldest source to the youngest one in NGC 7538. In general, Cep A showed highly polarized masers with weak linear polarization (typically a few per cent) but strong circular polarization (typically >50 per cent). The median m_t for 1665- and 1667-MHz features is 80 per cent. That confirms the young evolutionary stage of the Cep A region (similarly to the object IRS 11 in NGC 7538). There are no significant differences between the polarization properties of regions 2 and 3 what implies a similar age for all HII regions.

4.2.2 Decay of magnetic field

Cohen et al. (1990) monitored the Zeeman quartet at 1665- and 1667-MHz over a 10-year time span. They present evidence for a $0.4 \text{ per cent yr}^{-1}$ decay of the magnetic field strength in the OH maser region due to expansion of molecular gas surrounding a young star. In Fig. 6 we present

measurements of the velocity separations of the components of the Zeeman quartet over a longer period of 25 years. We include previously reported data from 1980–90 (Wouterloot et al. 1980; Cohen et al. 1990; Fish et al. 2003) and unpublished measurements taken with the Lovell antenna in the period 1990–95 (Cohen et al., in prep.). Our interferometric data gave separations between peaks of 1.9 km s^{-1} at 1665 MHz and 1.1 km s^{-1} at 1667 MHz in 1999. We also detected the Zeeman quartet with the Nançay antenna in 2002 October and 2004 September (Szymczak et al., in prep.). The velocity separations were then $1.952, 1.93 \text{ km s}^{-1}$ (at 1665 MHz) and $1.15, 1.11 \text{ km s}^{-1}$ (at 1667 MHz) in both epochs, respectively. Taking the whole 25-year period we used least-squares fits to estimate the rates of change in line splitting, obtaining $-0.0053 \pm 0.0006 \text{ km s}^{-1} \text{ yr}^{-1}$ for the 1665-MHz line and $-0.0013 \pm 0.0007 \text{ km s}^{-1} \text{ yr}^{-1}$ for the 1667-MHz line. The rates of change of field strength implied are $-0.009 \pm 0.001 \text{ mG yr}^{-1}$ from the 1665-MHz line and $-0.004 \pm 0.002 \text{ mG yr}^{-1}$ from the 1667-MHz line.

The two estimates for the magnetic field decay differ significantly of the 2.3σ level (3 per cent). This is also apparent in the lowest panel of Fig. 6. The ratio of line splitting should be 1.67 from theory whereas the observed ratios are 1.70–1.82. It is most likely those deviations are caused by blending (Sect. 3.3). In particular, 1665-MHz features C and c and 1667-MHz feature A all have similar velocities to the Zeeman quartet. It is impossible to correct data for this effect. We take the weighted mean of the 1665- and 1667-MHz results as our best estimate of the magnetic field decay. This gives a weighted mean of the magnetic field decay rate of $-0.0080 \pm 0.0009 \text{ mG yr}^{-1}$ which is $-0.24 \pm 0.03 \text{ per cent yr}^{-1}$.

5 CONCLUSIONS

We detected many new 1.6 GHz OH masers in the Cep A region, and confirm the strong variability of the OH maser emission. OH maser features around HII region 2 have an elongated E-W distribution, similar to that of the water masers. However, the OH maser kinematics do not show the regular position-velocity pattern seen in the water masers.

The most important result from our full polarimetry

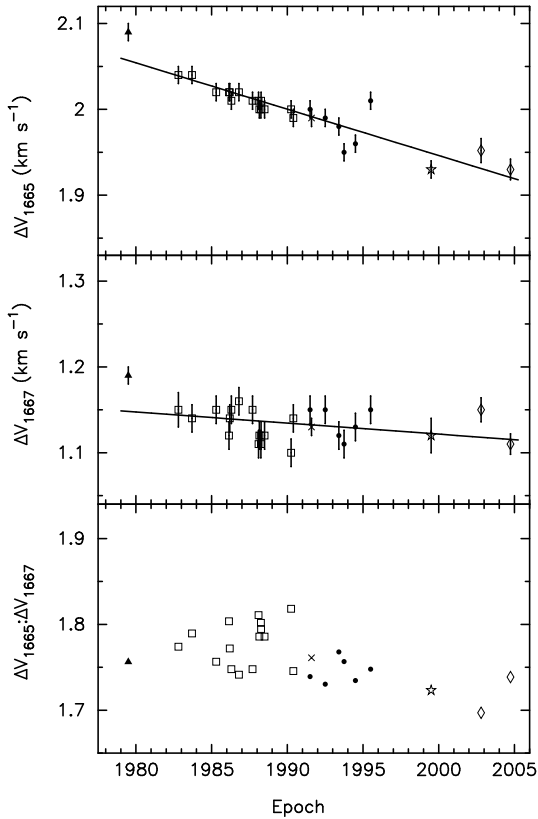


Figure 6. The systematic decrease of the magnetic field in Cep A shown by Zeeman quartet investigations. The open star represents data from this paper taken with MERLIN and diamonds represent data taken with the Nançay telescope in 2002 and 2004 (Szymczak et al., in prep.). The 1979 data are from Wouterloot et al. (1980) (triangle), the 1982–1990 data are from Cohen et al. (1990) (squares), the 1990–1995 data were taken with the Lovell antenna (Cohen, in prep.) (filled circles). A cross indicates the VLA data from Fish et al. (2003). Bars indicate errors in measurements. For the details of fitting see text.

observations is the morphology of magnetic field in close surroundings of the young stars. The Zeeman pairs reveal a reversal of the magnetic field direction on the arcsecond scale, pointed towards us in the west and away from us in the east. The electric vectors of linearly polarized features show an additional trend. Those from the outer parts of HII regions implied the direction of the magnetic field vector closely aligned with the interstellar magnetic field orientation derived from infrared polarimetry. In contrast, the vectors measured towards the central parts of HII regions were significantly rotated so as to be parallel to the radio jet (region 2). The Zeeman quartet showed a continuing systematic decrease of the magnetic field strength at a decay rate of -0.24 ± 0.03 per cent yr^{-1} . That is almost half the rate estimated previously (Cohen et al. 1990). However, there are also some effects of blending, which cannot easily be removed. Observations with higher angular resolution are needed in order to resolve features blended by MERLIN.

ACKNOWLEDGMENTS

We thank the referee, Prof. R. Crutcher, for helpful comments on this work, and thank Dr. J.-M. Torrelles for making

available continuum maps of Cep A and Prof. P.J. Diamond for the MFQUV files. MERLIN is a national facility operated by the University of Manchester at Jodrell Bank on behalf of PPARC. The work was supported by grant 2P03D01122 of the Polish State Committee for Scientific Research.

REFERENCES

- Argon A.L., Reid M.J., & Menten K.M., 2000, *ApJS*, 129, 159
- Bachiller R., 1996, *ARA&A*, 34, 111
- Blaauw A., Hiltner W.A., & Johnson H.L., 1959, *ApJ*, 130, 69
- Codella C., Bachiller R., Benedettini M., & Caselli P., 2003, *MNRAS*, 341, 707
- Cohen R. J., 1989, *Rep.Prog.Phys.*, 52, 881
- Cohen R.J., & Brebner G.C., 1985, *MNRAS*, 216, 51P
- Cohen R.J., Brebner G.C., & Potter M.M., 1990, *MNRAS*, 246, 3
- Cohen R.J., Rowland P.R., & Blair M.M., 1984, *MNRAS*, 210, 425
- Curiel S., Trinidad M.A., Canto J., Rodriguez L.F., Torrelles J.M., et al., 2002, *ApJ*, 564, L35
- Davies R.D., 1974, *Proc. IAU Sym.* 60, Kerr F., & Simonson S.C., 275
- Diamond P.J., Garrington S.T., Gunn A.G., Leahy J.P., McDonald A., Muxlow T.W.B., Richards A.M.S., & Thomasson P., 2003, *MERLIN User Guide*, ver. 3
- Fish V.L., Reid M.J., Argon A.L., & Menten K.M., 2003, *ApJ*, 596, 328
- Gallimore J.F., Cool R.J., Thornley M.D., & McMullin J., 2003, *ApJ*, 586, 306
- Garay G., Ramirez S., Rodriguez L.F., Curiel S., & Torrelles J.M., 1996, *ApJ*, 459, 193
- Gómez J.F., Sargent A.I., Torrelles J.M., Ho P.T.P., & Garay G., 1999, *ApJ*, 514, 287
- Gray M.D., Doel R.C., & Field D., 1991, *MNRAS*, 252, 30
- Gray M.D., Hutawarakorn B., & Cohen R.J., 2003, *MNRAS*, 343, 1067
- Hiriart D., Salas L., & Cruz-Gonzalez I., 2004, *AJ*, 128, 2917
- Hughes V.A., 2001, *ApJ*, 563, 919
- Hughes V.A., & Wouterloot J.G.A., 1984, *ApJ*, 276, 204
- Hutawarakorn B., & Cohen R.J., 1999, *MNRAS*, 303, 845
- Hutawarakorn B., & Cohen R.J., 2003, *MNRAS*, 345, 175
- Hutawarakorn B., & Cohen R.J., 2005, *MNRAS*, 357, 338
- Hutawarakorn B., Cohen R.J., & Brebner G.C., 2002, *MNRAS*, 330, 349
- Jones T.J., Woodward C.E., & Kelley M.S., 2004, *AJ*, 128, 2448
- Kudoh T., & Shibata K., 1997, *ApJ*, 474, 362
- Migenes V., Cohen R.J., & Brebner G.C., 1992, *MNRAS*, 254, 501
- Minier V., Booth R.S., & Conway J.E., 2000, *A&A*, 362, 1093
- Narayanan G., & Walker C.K., 1996, *ApJ*, 466, 844
- Niezurawska A., Szymczak M., Cohen R.J., & Richards A.M.S., 2004, *MNRAS*, 350, 1409
- Rodriguez L.F., Ho P.T.P., & Moran J.M., 1980, *ApJ*, 240, L149
- Sargent A.I., 1977, *ApJ*, 218, 736
- Sarma A.P., Troland T.H., Crutcher R.M., & Roberts D.A., 2002, *ApJ*, 580, 928
- Torrelles J.M., Gomez J.F., Garay G., Rodriguez L.F., Curiel S., Cohen R.J., & Ho P.T.P., 1998, *ApJ*, 509, 262
- Torrelles J.M., Gomez J.F., Rodriguez L.F., Curiel S., Ho P.T.P., & Garay G., 1996, *ApJ*, 457, L107
- Torrelles J.M., Patel N.A., Gomez J.F., Ho P.T.P., Rodriguez L.F., Anglada G., Garay G., Greenhill L., Curiel S., & Canto J., 2001, *ApJ*, 560, 853
- Torrelles J.M., Verdes-Montenegro L., Ho P.T.P., Rodriguez L.F., & Canto J., 1993, *ApJ*, 410, 202

- Uchida Y., & Shibata K., 1985, PASJ, 37, 515
Wardle J.F.C., & Kronberg P.P., ApJ, 194, 249
Ward-Thompson D., Kirk J.M., Crutcher R.M., Greaves J.S.,
Holland W.S., André P., 2000, ApJ, 537, L135
Wouterloot J.G.A., Habing H.J. & Herman J., 1980, A&A, 81,
L11